We are IntechOpen, the world's leading publisher of Open Access books Built by scientists, for scientists

4,800
Open access books available

122,000
International authors and editors

135M
Downloads

Our authors are among the

154
Countries delivered to

TOP 1%
most cited scientists

12.2%
Contributors from top 500 universities

CLARIVATE ANALYTICS BOOK CITATION INDEX INDEXED

WEB OF SCIENCE™

Selection of our books indexed in the Book Citation Index in Web of Science™ Core Collection (BKCI)

Interested in publishing with us?
Contact book.department@intechopen.com

Numbers displayed above are based on latest data collected.
For more information visit www.intechopen.com

5

Electrochemical Corrosion Behavior of Magnesium Alloys in Biological Solutions

Amany Mohamed Fekry
Cairo University (Faculty of Science)
Egypt

1. Introduction

Magnesium (Mg) is the fourth most abundant cation in the human body [Fekry & El-Sherief, 2009]. It is very abundant in the Earth being considered the fourth highest, following iron, oxygen and silicon. The raw ores of Mg are dolomite ($MgCO_3.CaCO_3$) and magnesite ($MgCO_3$), and Mg is the second most abundant metal in seawater following sodium. It is therefore a comparatively low cost material. Magnesium is the lightest of all metals in practical use, and has a density (1.74 g cm^{-3}) of about two thirds of aluminum and only one quarter that of iron. Pure magnesium metal has useful properties such as shielding against electromagnetic waves, vibration damping, dent resistance, machinability and low toxicity in humans, in addition to its recyclability as it has a lower specific heat and a lower melting point than other metals. On the other hand, magnesium has shortcomings such as insufficient strength, elongation and heat resistance as well as being subject to corrosion. To put Mg to practical use, it is necessary to deal with its shortcomings and improve its performance through alloying with various elements. Alloying magnesium improves its strength, heat resistance and creep resistance (creep is defined as deformation at a high temperature and under load). However, the addition of alloying elements modifies the corrosion behavior of magnesium in such a way that it can be beneficial or deleterious.

Some advantages of magnesium alloys are their high stiffness-to-weight ratio, great ease of machinability, good casting qualities suitable for high pressure die-casting, high damping capacity and good weldability under controlled atmosphere. Magnesium can form intermetallic phases with most alloying elements, the stability of this phase increases with the electronegativity of the other element [Kainer, 2003]. Aluminum (Al) had already become the most important alloying element for significantly increasing the tensile strength, specifically by forming the intermetallic phase $Mg_{17}Al_{12}$. Similar effects can be achieved with zinc (Zn) and manganese (Mn), while the addition of silver (Ag) leads to improve high-temperature strength. The identification of magnesium alloys is standardized worldwide in the ASTM norm; each alloy is marked with letters indicating the main alloy elements, followed by the rounded figures of each (usually two) weight in percentage terms. The last letter in each identification number indicates the stage of development of the alloy.

However, according to the elemental composition two major magnesium alloy systems are available to the designer. The first includes alloys containing 2 – 10 wt% Al, combined with minor additions of zinc and manganese. These alloys are widely available at moderate cost,

Abbreviation letter	Alloying element	Abbreviation letter	Alloying element
A	Aluminum	N	Nickel
B	Bismuth	P	Lead
C	Copper	Q	Silver
D	Cadmium	R	Chromium
E	Rare earths	S	Silicon
F	Iron	T	Tin
H	Thorium	W	Yttrium
K	Zirconium	Y	Antimony
L	Lithium	Z	Zinc
M	Manganese		

Table 1. ASTM codes for magnesium's alloying elements

and maintain their room-temperature mechanical properties up to 95^{o} to 120^{o} C. Beyond this, increase in temperature adversely affects mechanical properties and the corrosion properties deteriorate rapidly. The most important alloys of this group are AZ-, AM- and AS – Mg based systems. The second group consists of magnesium alloyed with various elements (rare earths, zinc, thorium, and silver) except aluminum, all containing a small but effective zirconium content that imparts a fine grain structure and thus improved mechanical properties. These alloys generally possess much better elevated-temperature properties, but they are more costly. The most important alloys of this group are ZE, HK and ZK [Kainer, 2003].

Magnesium alloys as potential biodegradable material provides both biocompatibility and suitable mechanical properties [Song, 2007]. Mg^{2+} is an essential element and present in large amounts in the human body. It is the fourth most abundant cation in the human body, with an estimated 1 mol of magnesium stored in the body of a normal 70 kg adult, with approximately half of the total physiological magnesium stored in bone tissue [Song & song, 2007]. The presence of magnesium in the bone system is beneficial to bone strength and growth. Magnesium alloys have specific density (1.74–2 g/cm^3) and Young's modulus (41–45 GPa) most close to those (1.8–2.1 g/cm^3, 3–20 GPa) of human body's bone. Therefore, in orthopedic and bone repairing or replacement applications magnesium alloys are particularly superior to any other metallic or polymer implants in terms of physical and mechanical properties, as the dissimilarity in Young's modulus between an implant and natural bone can result in stress shielding effects, leading to concentration of stress at the interface between the bone and implant reducing stimulation of new bone growth and decreasing implant stability [Song, 2007].

On the other side, magnesium is 1.6 and 4.5 times less dense than aluminum and steel, respectively. Moreover, magnesium is essential to human metabolism and is naturally found in bone tissue [Fekry & El-Sherief, 2009]. Biodegradable implant materials in the human body can be gradually dissolved, absorbed, consumed or excreted, so there is no need for the secondary surgery to remove implants after the surgery regions have healed. Metallic materials continue to play an essential role as biomaterials to assist with the repair or replacement of bone tissue that has become diseased or damaged. Thus, it is projected

that magnesium and its alloys be applied as lightweight, degradable, load bearing orthopedic implants, which would remain present in the body and maintain mechanical integrity over a time scale of 12–18 weeks while the bone tissue heals, eventually being replaced by natural tissue [Staiger et al., 2006]. Also, magnesium has a high negative standard electrode potential (−2.37 V at 25 °C) and thus is corroded relatively faster than other metallic materials, especially in Cl^- containing aqueous environment, indicating that magnesium can degrade/or be corroded in a human body environment. Thus interface problems such as interface loosening and inflammation can be resolved and the second removal surgical operation for the case of bone screws and plates can be avoided. Thus, Mg alloy can gradually be dissolved and adsorbed after implanting [Revell et al., 2004; Zreiqat et al., 2002; Yamasaki, 2002 & 2003]. A suitable degradation rate is critical to a biodegradable Mg implant before the tissue has been sufficiently recovered or healed [Witte, 2005]. After the recovery or healing, the implant should be gradually dissolved, consumed or absorbed by the human body. In fact, with recent developments and understandings of corrosion and prevention of Mg alloy, controlling the corrosion performance of Mg alloy should be possible now [Yamasaki, 2003; Song & Atrens, 2003]. Extruded Mg alloys as AZ91E and AZ31E are getting more and more widely used because of their considerably high plasticity in comparison with the die-cast Mg alloys [Zenner & Renner, 2002]. Several studies [Song, 2007; Witte et al. 2008; Song et al., 1999] have shown that the corrosion behavior of Mg alloys is significantly dependent on the alloying elements and the microstructure.

Glucosamine ($C_6H_{13}NO_5$) is an amino sugar. All of the glucosamine forms originated from shellfish**,** Some carrier molecules are needed (such as sulphate or HCl) because raw glucosamine is unstable by itself - it needs to be bound to the sulfate or HCl carrier in order to be stored for any period of time. Glucosamine sulfate is a naturally occurring chemical compound found in the human body. It is used by the body to produce a variety of other chemicals that are involved in building tendons, ligaments, cartilage, and the thick fluid that surrounds joints. Glucosamine sulfate used in dietary supplements does not always come from natural sources. It can also be made in a laboratory. Glucosamine sulfate is commonly used for arthritis. Scientists have studied it extensively for this use [Giordano et al., 2009].

Osteoarthritis (OA) is the most common form of arthritis that can affect the hands, hips, shoulders and knees. In OA, the cartilage that protects the ends of the bones breaks down and becomes thin. This results in more joint friction, pain, and stiffness. Researchers think that taking glucosamine supplements may either increase the cartilage and fluid surrounding joints or help to prevent breakdown of these substances, or may be both. Supplemental glucosamine may help to prevent cartilage degeneration and treat arthritis.

This chapter reviews the biological performance of magnesium based alloys (biodegradable materials for temporary implant) as AZ91D alloy in simulated body fluid (SBF), AZ31E alloy in Ringer's and AZ31E, AZ91E in Hank's solution at 37 ^oC that have been used as orthopedic biomaterials. Their corrosion behavior was studied by the analysis of corrosion resistance variation with immersion time, using electrochemical impedance spectroscopy (EIS) tests and corrosion current density using potentiodynamic polarization technique. The results were confirmed by scanning electron micrographs. The aim is to explore possible routes to improve limiting factors such as the corrosion resistance and improve integration of the implant with tissue, and ultimately highlights the need for further research. It is aimed to find the best magnesium alloy with low cost and low corrosion rate as implant in human body. Furthermore, the feasibility to slow down the biodegradation (i.e. corrosion)

of magnesium alloys to solve the rapidly corroding magnesium implant problems was demonstrated by studying the effect of adding glucosamine sulphate to Hank's solution on the corrosion behavior of AZ31 alloy. This line of research was still under consideration.

2. The main problem and how to solve?

Recently, a number of studies had been carried out to investigate the corrosion behavior of magnesium alloy in artificial physiological fluids. However, most of them were considering an Al containing Mg alloy [Witte et al. 2006]. Most alloying elements will dissolve into the human body during the magnesium alloy degradation. Magnesium alloys did not perform well due to inappropriately high corrosion rates [Song & Song, 2007]. The screws and plates made of these magnesium alloys corroded too quickly due to high impurities of the alloys and as a consequence, subcutaneous gas cavities appeared in treated patients [Song & Song, 2007]. However, slower corrosion rates are needed for magnesium alloys to be suitable as a potential biomaterial [Witte et al. 2005]. Mn and Zn were selected to develop a Mg–Zn–Mn magnesium alloy for biomedical application due to the good biocompatibility of Zn and Mn elements [Zhang et al. 2009]. The development of biodegradable implants is one of the most important research areas in medical science [Song & Song, 2007; Mani et al., 2007]. Compared with traditional permanent implants, biodegradable materials will not cause permanent physical irritation or chronic inflammatory discomfort. Mg or its alloys are non-toxic to the human body.

Thus in this study, it was observed that corrosion resistance for AZ91D in Simulated body fluid increase with increasing time of immersion until 35 h. Also, it found to increase for AZ31E in Ringer's solution increases with increasing immersion time till 100 h of immersion. Also, the corrosion resistance of AZ91E and AZ31E alloys increase with immersion time in Hank's solution for 100 h. However, the corrosion resistance of AZ31E alloy is much better than AZ91E alloy at all times of immersion. All results are confirmed by scanning electron micrographs. Also, by addition of Glucosamine as inhibitor for corrosion of AZ31E in Hank's solution, it was evaluated that total resistance R_T or relative thickness $1/C_T$ of the film formed are higher compared to the values in absence of glucosamine. However, the best corrosion inhibition is observed by addition of 0.01 mM Glucosamine and this was confirmed by SEM images.

3. Experimental

A die cast magnesium aluminum alloy (AZ91D) with composition (wt%): 9.0 Al, 0.67 Zn, 0.33 Mn, 0.03 Cu, 0.01 Si, 0.005 Fe, 0.002 Ni, 0.0008 Be and balance Mg, an extruded magnesium aluminum alloys with chemical composition (wt%): 2.8 Al, 0.96 Zn, 0.28 Mn, 0.0017 Cu, 0.0111 Fe, 0.0007 Ni, 0.0001 Be and balance Mg for AZ31E and 9.0 Al, 0.7 Zn, 0.13 Mn, 0.03 Cu, 0.01 Si, 0.006 Fe, 0.004 Ni, 0.0007 Be and balance Mg for AZ91E. All donated from Department of mining, Metallurgy and Materials Engineering, Laval University, Canada. The sample was divided into small coupons. Each coupon was welded to an electrical wire and fixed with Araldite epoxy resin in a glass tube leaving cross-sectional area of the specimen 0.2 cm^2 for AZ91D alloy and 0.196 cm^2 for both AZ91E and AZ31E alloys. The solutions used were simulated biological fluid (SBF), recommended by Cigada, which contains (g/l): NaCl 8.74, $NaHCO_3$ 0.35, Na_2HPO_4 0.06, NaH_2PO_4 0.06 [Fekry & El-

Sherief, 2009], Ringer's solution (RS) (g/l): NaCl 8.6, $CaCl_2$ 0.33, KCl 0.3, Hank's balanced salt solution with composition (g/l): NaCl 8.00, $NaHCO_3$ 0.35, Na_2HPO_4 0.0477, KH_2PO_4 0.06, KCl 0.40, D-Glucose 1.0 [Ghoneim et al., 2010]. The pH of the solution was 7.4. Glucosamine sulphate $(C_6 H_{14} NO_5)_2SO_4.2KCl$ and all solutions are prepared using triply distilled water. The surface of the test electrode was mechanically polished by emery papers with 400 up to 1000 grit to ensure the same surface roughness, degreasing in acetone, rinsing with ethanol and drying in air. The cell used was a typical three-electrode one fitted with a large platinum sheet of size 15×20×2mm as a counter electrode (CE), saturated calomel (SCE) as a reference electrode (RE) and the alloy as the working electrode (WE). The impedance diagrams were recorded at the free immersion potential (OCP) by applying a 10 mV sinusoidal potential through a frequency domain from 100 kHz down to 100 mHz. The EIS was recorded after reading a steady state open-circuit potential. The polarization scans were carried out at a rate of 1 mV/s over the potential range from -2.5 to 0 mV vs. saturated calomel electrode (SCE). Prior to the potential sweep, the electrode was left under open-circuit in the respective solution until a steady free corrosion potential was recorded. Corrosion current, i_{corr}, which is equivalent to the corrosion rate is given by the intersection of the Tafel lines extrapolation. In the weight loss measurements, the treated samples were weighed before and after the immersion in Hank's solution in absence and in presence of different concentrations of glucosamine sulphate. The instrument used is the electrochemical workstation IM6e Zahner-elektrik, GmbH, (Kronach, Germany).The electrochemical and weight loss experiments were always carried inside an air thermostat which was kept at 37^{o}C, unless otherwise stated. The SEM micrographs were collected using a JEOL JXA-840A electron probe microanalyzer.

4. Results and discussion

4.1 Electrochemical impedance measurements

4.1.1 AZ91D alloy in simulated body fluid (SBF)

The EIS scans as Bode plots in Fig. 1a-c. for AZ91D alloy in dependence on the immersion time were recorded in the test solution for 35 h. The diagrams show resistive regions at high and low frequencies and capacitive contribution at intermediate frequencies. The impedance (|Z|) as well as the phase shift (θ) of AZ91D alloy is clearly found to depend on immersion time. It is of inertest to observe that an increase in time of immersion, from 0 to 1.5 h (Fig. 1a), continuously increases the |Z| value whilst θ_{max} is nearly constant.

However, at 2.0 to 10 h (Fig. 1b), the impedance value increases but not sharply. At higher immersion time 15-35 h (Fig. 1c), an increase in the immersion time increases the |Z| value whilst θ_{max} gradually decreases with a concomitant shift to lower frequencies. This trend is most likely a result of a decrease in the surface film capacitance commensurate with a decrease in the adsorbed amount of anions forming SBF as Cl^-, HCO_3^-, $H_2PO_4^-$ or HPO_4^{-2} on the electrode surface [Fekry & El-Sherief, 2010]. The results in general reveal two clear trends concerning the number of peaks observed in the patterns of the phase shift. The first one is for the behavior of AZ91D alloy at time of immersion from 0 to 5 h, where the Bode plots display only one maximum phase lag (Fig. 1a, b). The second trend is for the alloy at immersion time from 10 to 35 h where another peak of phase lag appears at the low frequency region (Fig. 1c).

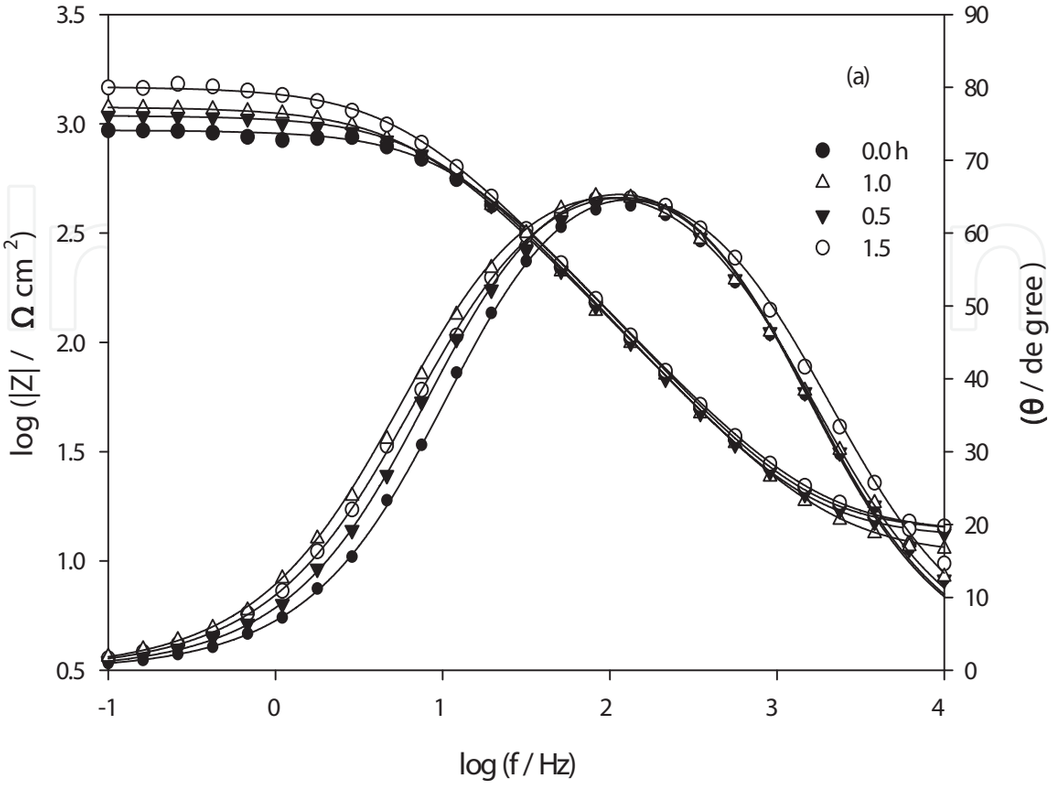
(a)
0.0 h
1.0
0.5
1.5
log (|Z| / Ω cm 2)
(θ / de gree)
log (f / Hz)

(a)

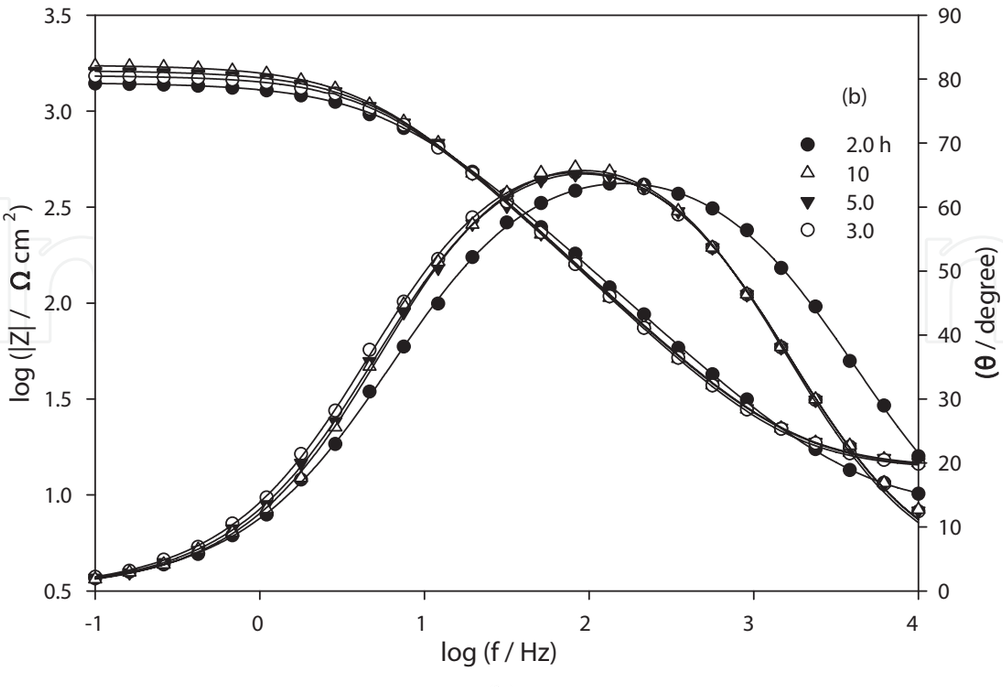
(b)
2.0 h
10
5.0
3.0
log (|Z| / Ω cm 2)
(θ / degree)
log (f / Hz)

(b)

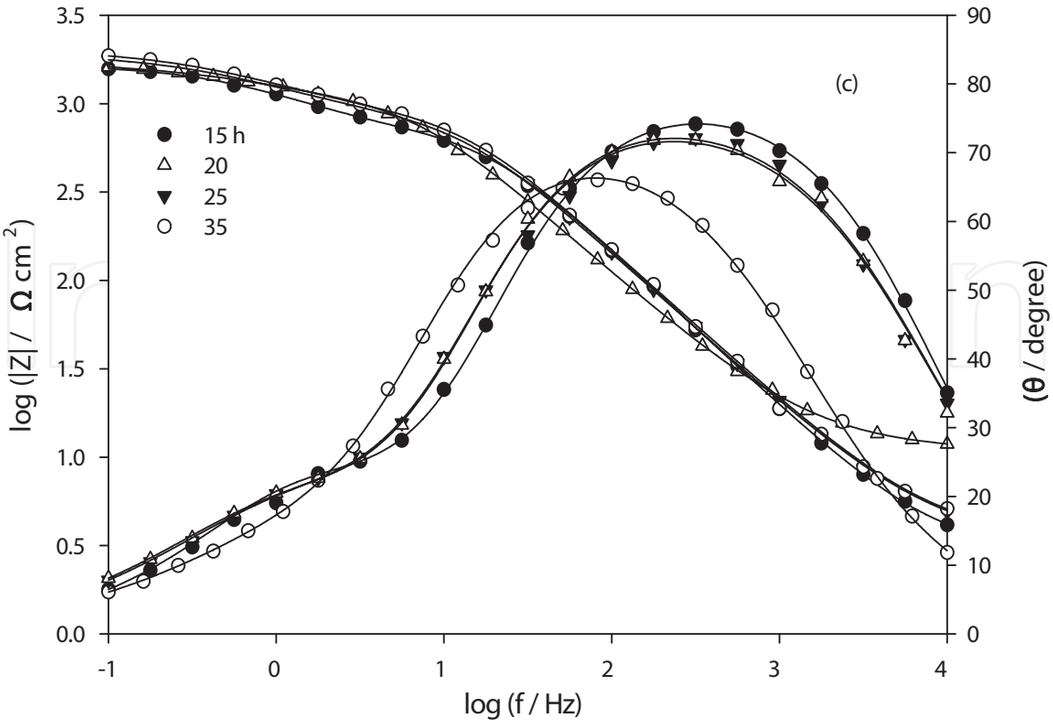

(c)

Fig. 1. a-c. Bode plots of AZ91D alloy as a function of immersion time in SBF at 37 °C.

The impedance data were thus simulated to the appropriate equivalent circuit for the cases with one time constant (Fig. 2a) and the others exhibiting two time constants (Fig. 2b), respectively. This is the simulation that gave a reasonable fit using the minimum amount of circuit components. Generally, the impedance response of an actively corroding metal in an aqueous solution is well simulated by the classic parallel resistor capacitor (R_1C_1) combination in series with the solution resistance (R_s) between the specimen and the RE. In this model a charge transfer resistance (R_1) is in parallel with the double layer capacitance (C_1), as depicted in Fig. 2a. In this case, the electrode surface is covered with a passive film R_1 and C_1, the film resistance and capacitance, respectively. On the other hand, for the impedance diagrams with two time constants the appropriate equivalent model consists of two circuits in series from R_1C_1 and R_2C_2 parallel combination and the two are in series with R_s. In this way C_1 is related to contribution from the capacitance of the outer layer and the faradaic reaction therein and C_2 pertains to the inner layer, while R_1 and R_2 are the respective resistances of the outer and inner layers constituting the surface film, respectively [Wu et al., 2008]. Analysis of the experimental spectra were made by best fitting to the corresponding equivalent circuit using Thales software provided with the workstation where the dispersion formula suitable to each model was used [Fekry, 2009]. In this complex formula an empirical exponent (α) varying between 0 and 1, is introduced to account for the deviation from the ideal capacitive behavior due to surface inhomogeneties, roughness factors and adsorption effects [Fekry, 2009]. In all cases, good conformity between theoretical and experimental was obtained for the whole frequency range.

The experimental values are correlated to the theoretical impedance parameters of the equivalent model shown in Fig. 3. It was found that film healing and thickening (R_T) becomes effective by increasing time of immersion in SBF solution leading to a quasi-steady state thickness at longer times ($1/C_T$). This is caused by the formation of adherent corrosion products on the sample surface as $Mg(OH)_2$ which is precipitated from the solution during the corrosion of magnesium alloys due to saturation and localized alkalization [Gu et al., 2009]. Metal ions released from corrodible alloys to the surrounding tissues, may cause

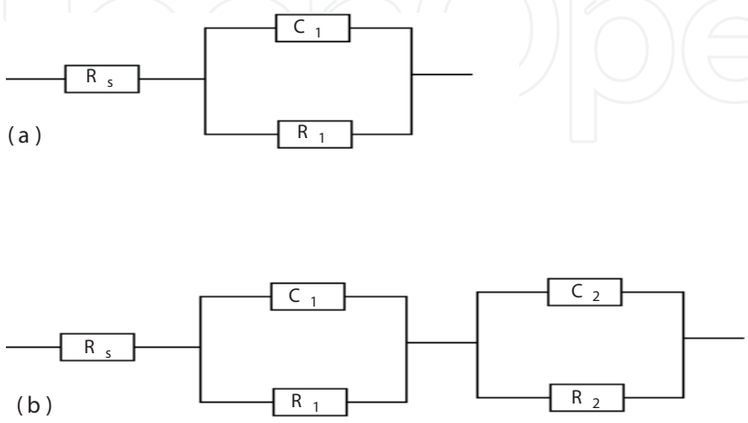

Fig. 2. Equivalent circuit model representing (a) one, and (b) two time constants for an electrode/electrolyte solution interface.

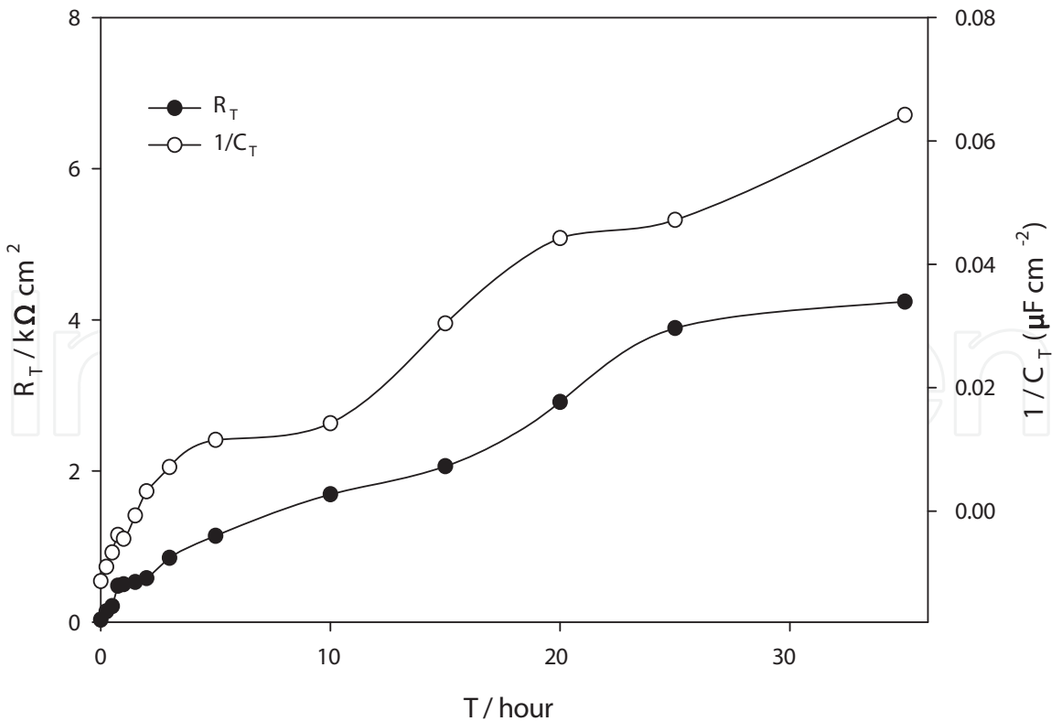

Fig. 3. The total resistance (R_T) and relative thickness ($1/C_T$) for AZ91D alloy as a function of immersion time in SBF at 37 °C.

biological responses in short term or prolonged periods. The toxicity of a metallic material is governed not only by its composition and toxicity of the component elements but also by its corrosion and wear resistance [Gu et al., 2009]. In a saline environment, magnesium-based alloys would be degraded to magnesium chloride, oxide, sulphate or phosphate [Fekry & El-Sherief., 2009] and the same occur in SBF. Also, magnesium carbonate precipitated on the surface of magnesium alloy improved the corrosion resistance of magnesium alloy in the case of atmospheric corrosion [Jönsson et al., 2007]. For chloride ions, in poorly buffered chloride solutions, they reveal low corrosion rates due to the formation of a partially protective $Mg(OH)_2$ layer. Also, phosphates inhibit dissolution of the oxide film and raise the corrosion potentials with increasing immersion time [Narayanan & Seshadri, 2007]. Phosphate is formed on the oxide surface and prevents dissolution. Generally, SBF improves slightly the corrosion resistance of AZ91D alloy with time.

It should be also emphasized that formation of a complete surface layer of oxidation products looks to be very difficult. This can be confirmed by SEM examination of AZ91D alloy surface after 35 h immersion in the respective SBF (pH 7.4) as shown in Fig. 4 compared to that of the polished sample (blank) at magnifications of 1000x. As can be seen, the micrograph for blank consists from uniform distribution, however, after immersion; it shows microcracks [Heakal et al., 2009 & 2009] which determine the existence of film vulnerable region. The relatively fine β-phase ($Mg_{17}Al_{12}$) precipitated at the outer portions of the platelets has light appearance with a shiny white color. However, flower-like $MnAl_2$ intermetallic inclusions [Pardo et al., 2008] are also found deposited on some few areas from the surface.

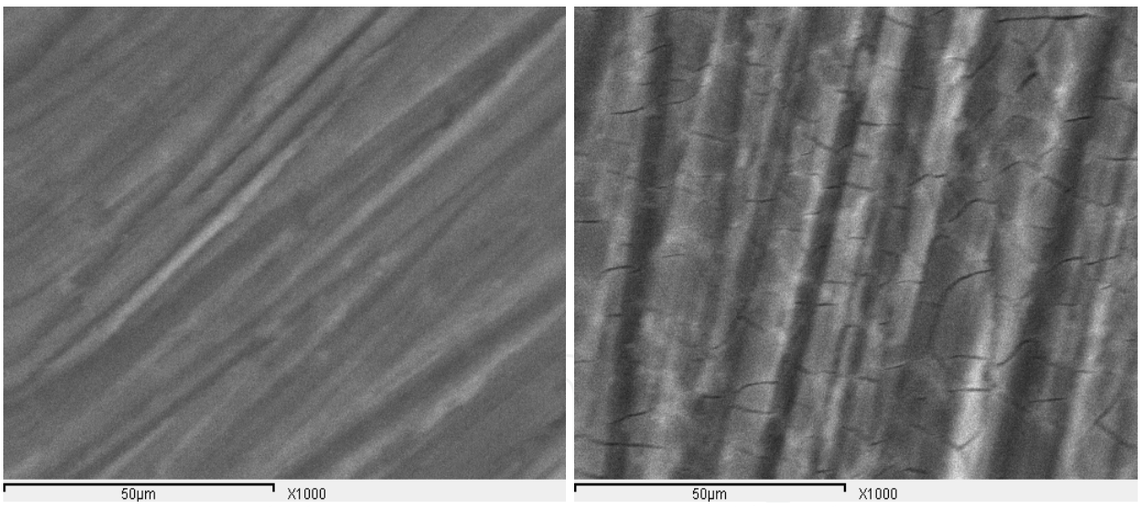

Blank After 35 h immersion

Fig. 4. SEM images of AZ91D alloy in air after polishing (blank) and in SBF at 37 °C after 35 h of immersion.

4.1.2 AZ31E alloy in Ringer's Solution (RS)

The EIS scans as Bode plots, in Fig. 5a-c, for AZ31E alloy, as function of the immersion time, were recorded in the test solution for 100 h. The diagrams show resistive regions at high frequencies. The impedance (|Z|) as well as the phase shift (θ) of AZ31E alloy is clearly dependent on immersion time. It is of inertest to observe that an increase in the time of

immersion, from 0 to 4.0 h (Fig. 5a), gradually increases the |Z| value, whereas θ_{max} is nearly constant. From 8.0 to 20 h (Fig. 5b), the impedance and θ_{max} values increase gradually. For larger immersion time from 30-70 h (Fig. 5c), both |Z| value and θ_{max} increase sharply. The results in general show that Bode plots display two maximum phase lags. Fig. 6, as an example for 1h immersion of AZ31E alloy, manifested two depressed capacitive semicircles, typical of Randles element, at higher and lower frequencies regions, separated by an inductive loop at intermediate frequencies. Inductive loops can be explained by the occurrence of an adsorbed intermediate on the surface. The experimental data were consistent with the involvement of the intermediate species Mg^+ in magnesium dissolution at film imperfections or on a film-free surface. At such sites, magnesium is first oxidised electrochemically to the intermediate species Mg^+, and then the intermediate species react chemically with water to produce hydrogen and Mg^{2+}. The presence of Cl^- ions increases the film free area, and accelerates the electrochemical reaction rate from magnesium metal to Mg^+ [Song et al., 1997]. The capacitive semicircle at higher frequencies is attributed to the redox $Mg–Mg^+$ reaction since it was assumed to be the rate determining step in the charge transfer process. Therefore, the resistance value obtained from intercepts of the first capacitive semicircle with real axis corresponds to the charge transfer resistance. On the other hand, the second capacitive semicircle could be attributed to the fast complementary corrosion reaction. The curve manifested that addition of chloride ions leads to increase in the size of the capacitive semicircles with immersion time, an indication of increasing the resistances and decreasing the corrosion rate. The increase in resistivity arises from the change in chemical composition of the surface film due to incorporation of Cl^- ions into the film especially through defect sites with low ionic resistance.

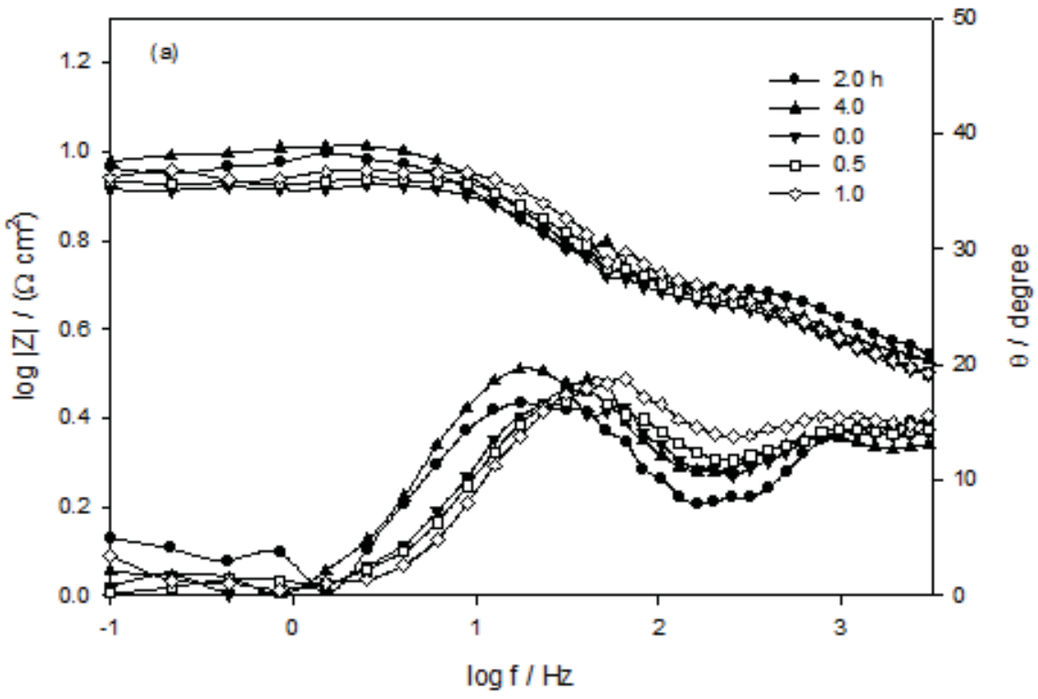

(a)

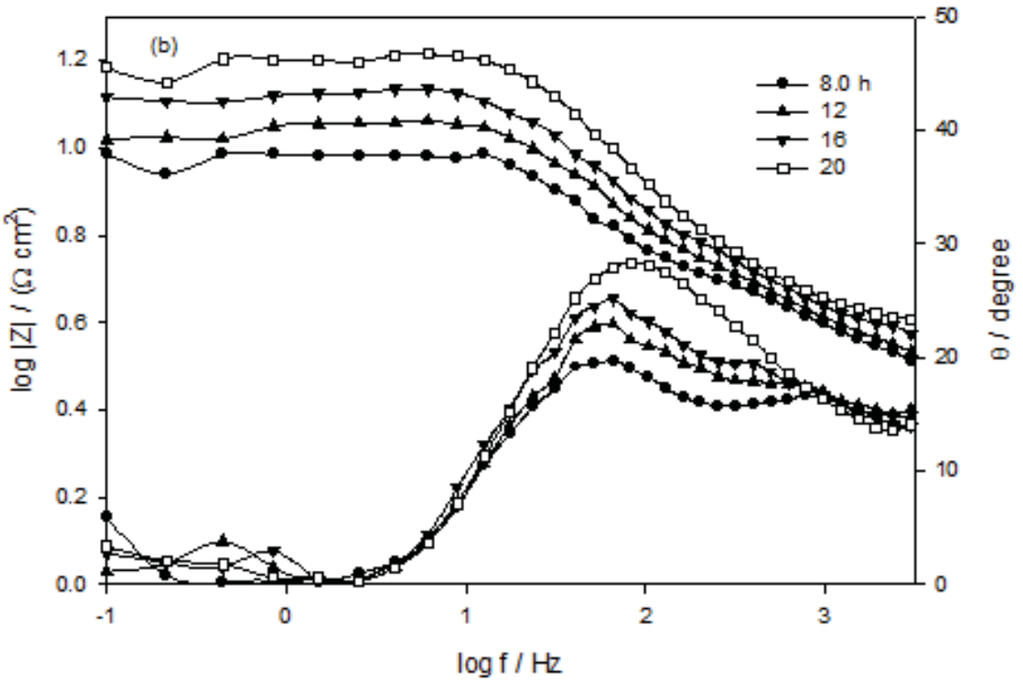

(b)

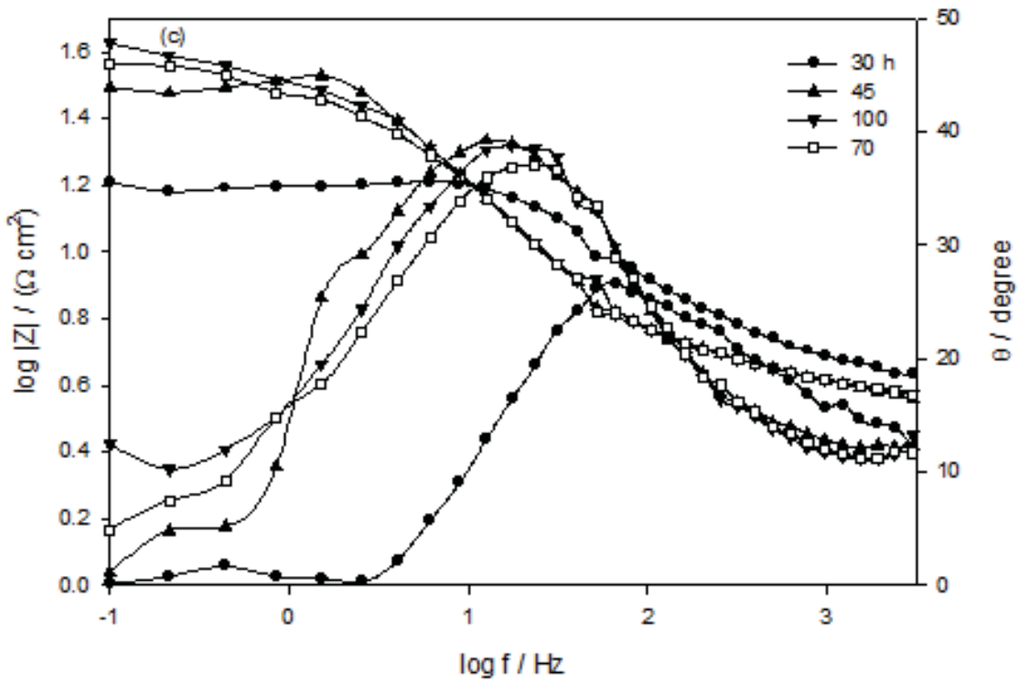

(c)

Fig. 5. a-c. Bode plots of AZ31E alloy as a function of immersion time in RS at 37 °C.

The impedance data were thus simulated to the appropriate equivalent circuit for the case with two time constants (Fig. 7). The model includes the solution resistance R_s, a series combination of resistance, R, and inductance, L, in parallel with charge transfer resistance $(R_{ct})_1$, and the constant phase element (CPE_1). In the high frequency limit, the inductive contribution to the overall impedance is insignificant. Therefore, the Nyquist plot of the impedance is a semicircle characteristic of the parallel arrangement of the double layer capacitance and charge transfer resistance corresponding to the corrosion reaction. Contribution to the total impedance at intermediate frequencies comes mainly from the charge transfer resistance and inductive component in parallel. The inductor arising from adsorption effects could be defined as ($L = R\tau$) , where τ is the relaxation time for adsorption on the electrode surface. The low frequency locus displays the characteristics of parallel RC circuit. This circuit includes another constant phase element (CPE_2) which is placed in parallel to charge transfer resistance element $(R_{ct})_1$. The $(R_{ct})_1$value is a measure of charge transfer resistance corresponding to the Mg^{+}–Mg^{2+} reaction. The CPE is used in this model to compensate for non-homogeneity in the system and is defined by two values, Q and a.

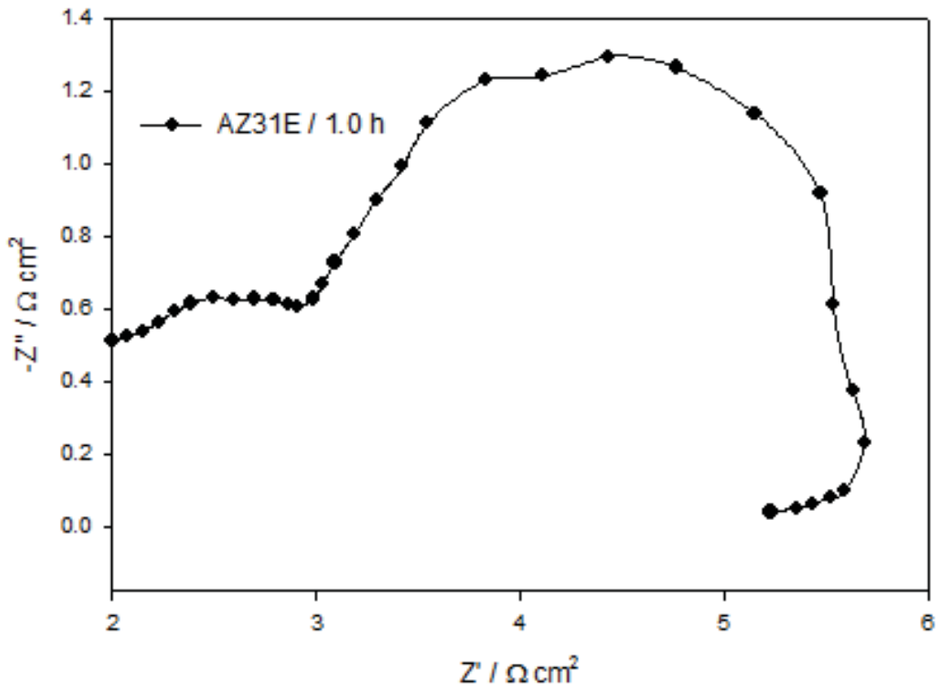

Fig. 6. Nyquist plot after 1 h of immersion in RS at 37 ◦C.

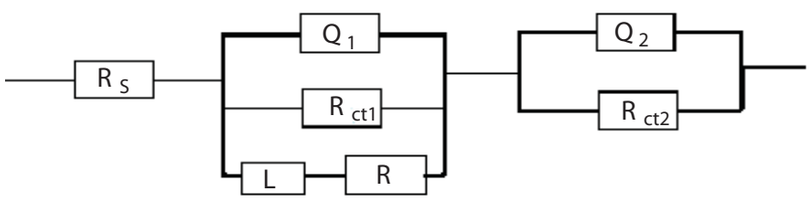

Fig. 7. Equivalent circuit model representing two series time constants for an electrode/electrolyte solution interface.

The impedance of CPE is represented by $Z_{CPE} = Q^{-1}(i\omega)^{-a}$, where $i = (-1)^{1/2}$, ω is frequency in rad s^{-1}, $\omega = 2\pi f$ and f is the frequency in Hz. If a equals one, the impedance of CPE is identical to that of a capacitor, $Zc = (i\omega C)^{-a}$ and in this case Q gives a pure capacitance (C). For non-homogeneous systems, a values range from 0.9–1. Computer fitting of the spectrum allows evolution of the elements of the circuit analogue. The aim of the fitting procedure is to find those values of the parameters which best describe the data. The experimental and computer fit results are given in Table 2. It was found that the fit results were consistent with the experimental data within 5% error.

As shown in Table 2, film healing and thickening becomes effective by increasing the time of immersion in Ringer's solution, leading to a quasi-steady state thickness at longer times. This is caused by the formation of adherent corrosion products on the sample surface as $Mg(OH)_2$ which is precipitated from the solution during the corrosion of magnesium alloys due to saturation and localized alkalization [Fekry & El-Sherief, 2009]. This is confirmed by measuring the pH of Ringer's solution after completing the experiment, which becomes 11.0. Calcium could improve both the corrosion resistance in NaCl solution and the mechanical properties of magnesium alloy. Moreover, Ca is a major component in human bone and can accelerate the bone growth [Azza et al., 2010]. It was thought that the presence of Ca ion benefits the bone healing. However, for chloride ions, low corrosion rates were obtained due to the formation of a partially protective $Mg(OH)_2$ layer. The growth of the polarization resistance with the immersion time is consistent with the continual decrease of the bio-corrosion rate.

SEM examination of AZ31E alloy surface after 100 h immersion in the same RS is shown in Fig. 8, as compared to that of the uniform distribution for polished sample (blank). After immersion; it shows microcracks [Fekry & El-Sherief, 2009], which indicate the existence of a vulnerable film. There are plenty of visible corrosion products on the surface of AZ31 after 100 h immersion.

Time Hour	R_s / Ω cm^2	$(R_{ct})_1$ / Ω cm^2	Q_1 / μF cm^{-2}	α_1	R / Ω cm^2	L	$(R_{ct})_2$ / Ω cm^2	Q_2 / μF cm^{-2}	α_2
0.00	0.18	5.29	416.9	0.98	53.45	0.032	5.40	154.3	0.94
0.50	0.18	5.31	311.2	0.98	54.90	0.035	5.67	90.05	0.94
1.00	0.18	5.32	299.3	0.96	56.27	0.040	5.89	89.13	0.95
2.00	0.18	5.32	172.1	0.97	60.49	0.044	6.01	86.79	0.97
4.00	0.18	5.33	161.9	0.97	67.35	0.051	6.29	81.07	0.96
8.00	0.19	5.35	157.7	0.99	73.36	0.055	7.34	72.45	0.93
12.00	0.19	5.37	147.6	0.99	86.83	0.059	8.37	69.95	0.95
16.00	0.19	5.38	146.9	0.98	105.2	0.061	9.01	55.87	0.94
20.00	0.19	5.38	143.8	0.99	106.2	0.061	9.06	45.21	0.98
30.00	0.22	6.37	139.8	0.99	248.3	0.145	24.9	41.14	0.97
45.00	0.39	6.40	135.5	0.98	258.7	0.147	25.1	30.30	0.97
70.00	0.58	6.45	132.8	0.99	307.5	0.151	30.6	17.15	0.97
100.00	0.59	6.53	116.3	0.99	405.1	0.154	36.8	14.23	0.98

Table 2. Impedance parameters of AZ31E alloy in RS at 37 °C.

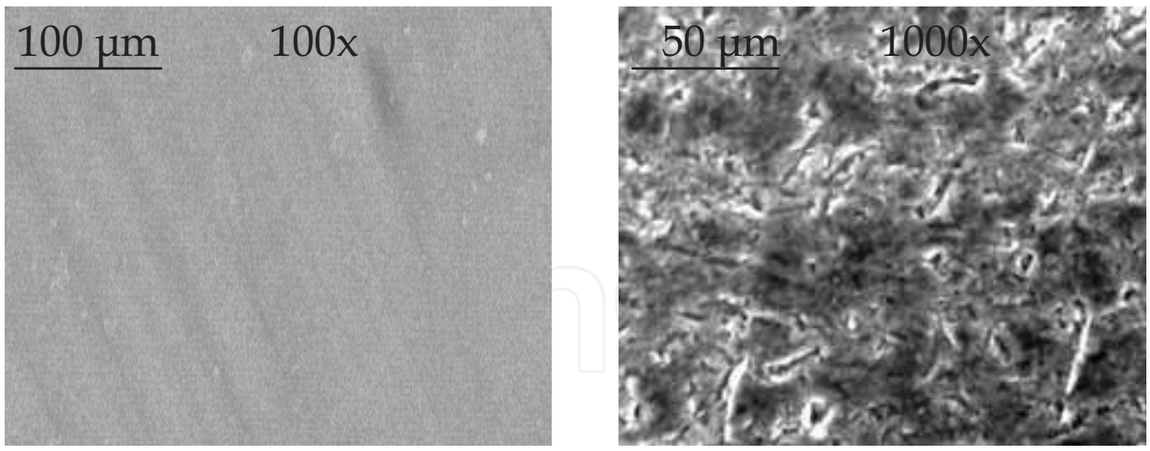

before immersion after 100 h immersion

Fig. 8. SEM images of (a) Ti-6Al-4V alloy and (b) AZ31E in air after polishing (blank) and in RS at 37 ^{o}C after 100 h of immersion.

4.1.3 AZ31E and AZ91E alloy in Hank's Solution (HS)

Electrochemical impedance (EIS) is a technique with small perturbative signal and the surface damage of the sample is very little. In these experiments, the immersion of the two magnesium alloys was carried out continuously in Hank's solution which is used to simulate the biochemical reaction of the magnesium alloys in human physiological conditions. The specimens were suspended in Hank's solution up to 100 hour. The EIS scans as Bode plots at different immersion times are given in Fig. 9 (a,b) & 10 (a,b) for AZ31and AZ91 respectively. It can be seen that these diagrams for both alloys show resistive regions at high and low frequencies and capacitive contribution at intermediate frequencies. It is of interest to observe that an increase in time of immersion, from 0 to 10 h (Fig. 9a) for AZ31E and (Fig. 10a, b) for AZ91E, continuously increases the $|Z|$ and θ values. That is, as shown in (Fig. 9), θ_{max} increases with time from 26^{o} at 0 h to 65^{o} at 10 h of immersion for AZ31E alloy. However, at higher immersion time from 20 to 100 h (Fig. 9b) for AZ31E, the impedance value increases and θ_{max} value gradually decreases but not sharply (from ~ 65^{o} to 58^{o}) with a concomitant shift to lower frequencies. For AZ91E alloy (Fig. 10), θ_{max} increases with time from 22^{o} at 0 h to 28^{o} at 100 h of immersion that is nearly constant. However, at any immersion time the values of $|Z|$ or θ_{max} is always higher for AZ31E alloy as compared to AZ91E alloy, suggesting that AZ31E alloy is much more passive than AZ91E alloy in the test solution. Also $|Z|$ values increase with increasing immersion time for both tested alloys as shown in Fig. 9 and 10. This trend is due to a decrease in the surface film capacitance which is directly proportional to the decrease in the adsorbed amount of aggressive anions as Cl^{-} [Heakal et al., 2009].

The Bode format of Fig. 9&10 confirms the presence of two time constants as there are two maximum phase lags appears at medium frequencies (MF), and low frequencies (LF). On the other hand, for the impedance diagrams with two time constants the appropriate equivalent model, shown in Fig. 2b, is the most appropriate one. Analysis of the experimental spectra was made by best fitting to the corresponding equivalent circuit using Thales software provided with the workstation where the dispersion formula suitable to each model was used [Fekry & El-Sherief, 2009].

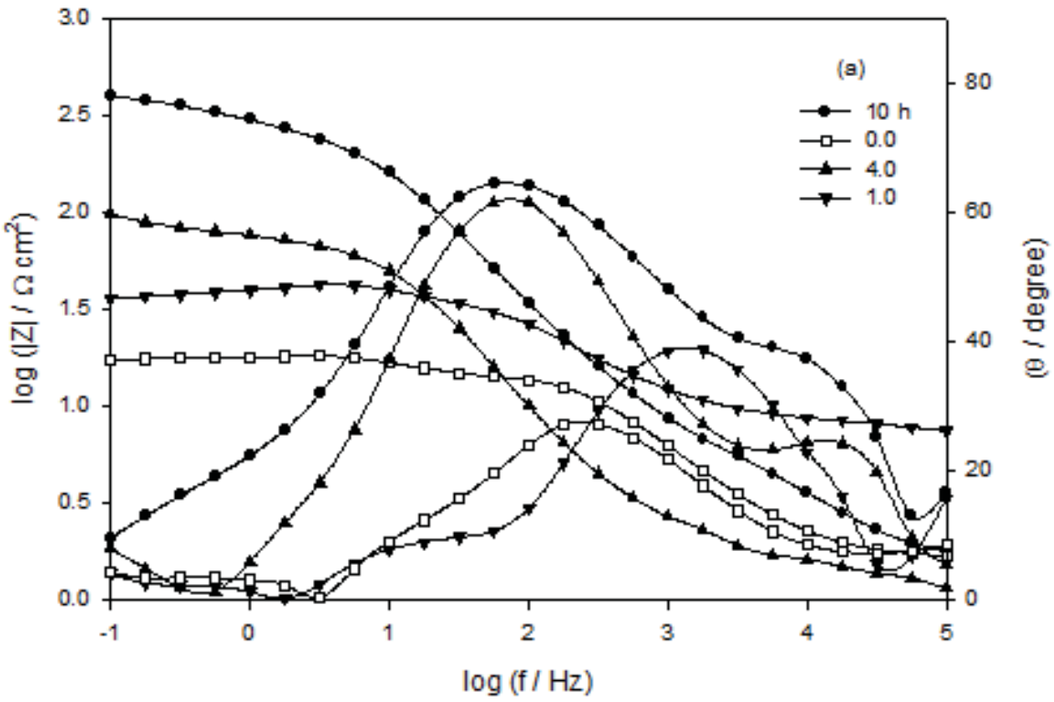

(a)

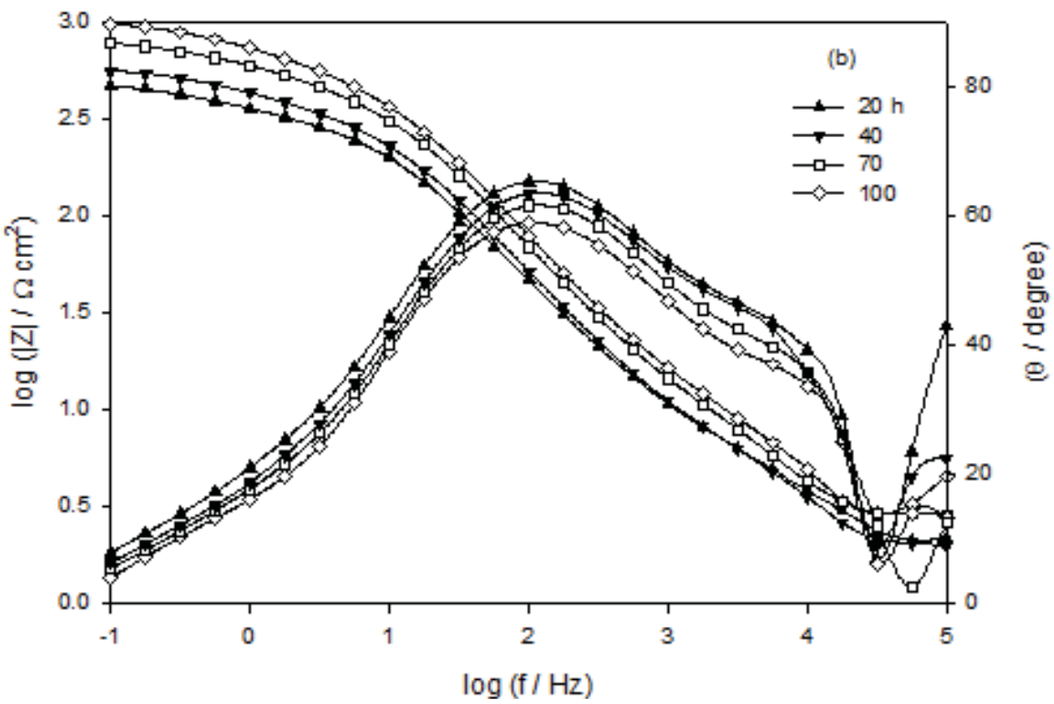

(b)

Fig. 9. a,b. Bode plots of AZ31E alloy as a function of immersion time in Hank's solution at 37 °C.

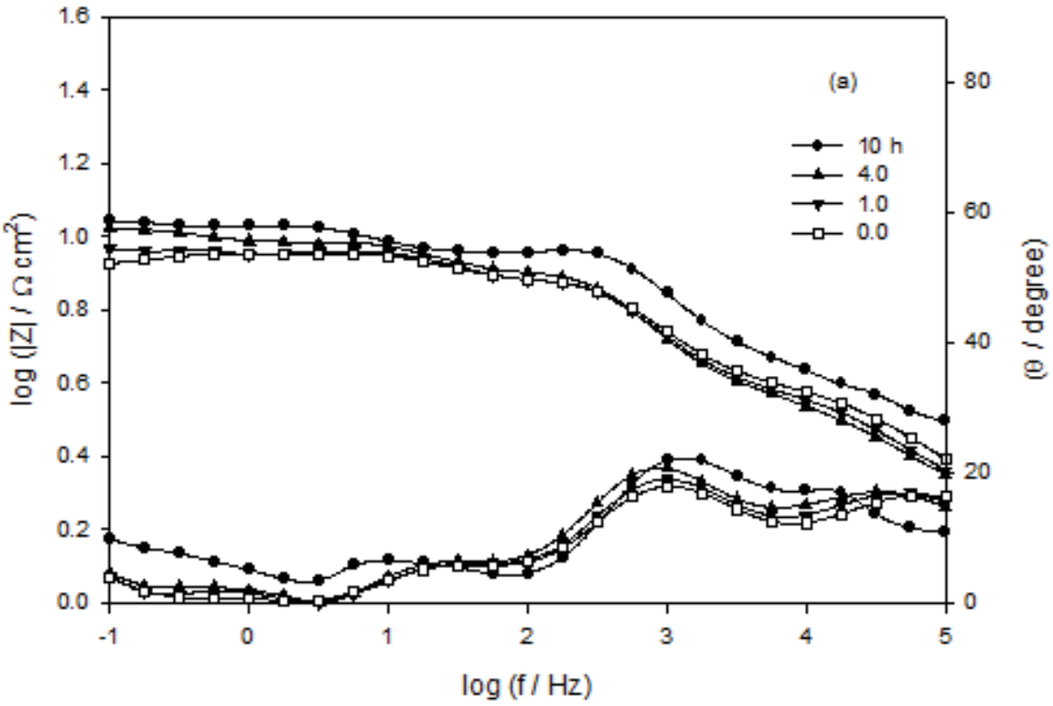

Fig. 10. a,b. Bode plots of AZ91E alloy as a function of immersion time in Hank's solution at 37 °C.

For this model the electrode impedance is represented by the following transfer function [Ameer et al., 2009]:

$$Z(\omega) = R_o + \frac{R_1}{1 + R_1 C_1 (j\omega)^{\alpha_1}} + \frac{R_2}{1 + R_2 C_2 (j\omega)^{\alpha_2}} \quad (1)$$

The above formula takes into account the deviation from the ideal RC behavior and considers, for a more realistic approach that each oxide layer as non-homogeneous. Thereby, the impedance associated with the capacitance of each layer is described by a constant phase element (CPE).

In all cases, good conformity between theoretical and experimental was obtained for the whole frequency range with an average error of 3%. The experimental values are correlated to the theoretical impedance parameters of the equivalent model, the data were presented in Tables 3&4 for AZ31E and AZ91E alloys, respectively. As given in Tables 3&4, R_s is nearly the same for both alloys. It was also seen that R_1, R_2 values increases and C_1, C_2 values decreases for both tested alloys with immersion time, that is film healing and thickening becomes effective by increasing time of immersion in Hank's solution leading to a quasi-steady state thickness at longer times. This is caused by the formation of adherent corrosion products on the sample surface including, magnesium hydroxide, as well as phosphates and carbonates [Wang et al., 2008]. They are precipitated from the solution during the corrosion of magnesium alloys due to saturation and localized alkalization [Gu et al., 2009]. Metal ions released from corrodible alloys to the surrounding tissues may cause biological responses in short term or prolonged periods. The toxicity of a metallic material is governed not only by its composition and toxicity of the component elements but also by its corrosion and wear

resistance [Gu et al., 2009]. In a saline environment, magnesium-based alloys would be degraded to magnesium chloride, oxide, sulphate or phosphate [Fekry & El-Sherief, 2009] and the same occur in Hank's solution. Also, magnesium carbonate precipitated on the surface of magnesium alloy improved the corrosion resistance of magnesium alloy in the case of atmospheric corrosion. For chloride ions, in poorly buffered chloride solutions, they reveal low corrosion rates due to the formation of a partially protective $Mg(OH)_2$ layer. Also, phosphates formed on the oxide surface inhibit dissolution of the oxide film with increasing immersion time [Narayanan & Seshadri, 2007]. For the values of the empirical exponent (α) given in Tables 3 & 4, it is seen that it is higher for AZ31E (~ 0.88 - 0.93) than that of AZ91E (~ 0.71 - 0.79) alloy. It is near to the ideal value (α = 1) for AZ31E alloy. Also, as given in Tables 3 & 4, R_1 or R_2 values at any given time is higher for AZ31E alloy than that for AZ91E alloy. This confirms that AZ31E is more resistant than AZ91E alloy in Hank's solution. Generally, Hank's solution improves slightly the corrosion resistance of AZ91E and AZ31E alloys with time.

Time hour	R_s / Ω cm²	R_1 / Ω cm²	C_1 / μF cm^{-2}	α_1	R_2 / Ω cm²	C_2 / μF cm^{-2}	α_2
0.00	2.21	2.10	90.3	0.88	17.9	24.7	0.88
0.25	2.20	2.14	87.5	0.89	22.5	23.5	0.89
0.50	1.97	2.32	81.3	0.89	25.2	22.2	0.88
1.00	2.10	2.38	78.5	0.87	40.3	21.8	0.90
4.00	2.15	9.66	71.4	0.87	105.4	19.2	0.90
10.00	2.65	37.77	67.1	0.91	482.3	18.7	0.89
20.00	2.85	65.18	65.8	0.89	584.9	17.8	0.92
40.00	2.42	82.11	63.9	0.91	667.9	17.1	0.92
70.00	2.61	126.23	61.7	0.91	867.7	16.7	0.92
100.00	3.00	197.35	59.0	0.90	985.0	16.4	0.93

Table 3. Impedance Parameters of AZ31E alloy in Hank's solution at 37°C.

Time hour	R_s / Ω cm²	R_1 / Ω cm²	C_1 / μF cm^{-2}	α_1	R_2 / Ω cm²	C_2 / μF cm^{-2}	α_2
0.00	2.60	1.04	150.8	0.75	8.5	50.3	0.71
0.25	2.03	1.16	143.1	0.78	8.7	47.8	0.74
0.50	1.91	1.25	135.6	0.76	8.8	43.2	0.75
1.00	1.82	1.47	122.0	0.78	11.0	35.5	0.72
4.00	1.27	1.64	117.1	0.75	11.8	32.1	0.72
10.00	2.65	1.79	111.0	0.77	13.8	29.9	0.75
20.00	2.67	1.99	105.5	0.76	15.7	27.5	0.75
40.00	2.71	2.13	101.3	0.77	18.2	25.1	0.74
70.00	2.69	2.18	97.1	0.76	32.6	21.4	0.72
100.00	2.03	2.55	85.7	0.79	43.1	21.0	0.74

Table 4. Impedance Parameters of AZ91E alloy in Hank's solution at 37°C.

It should be noted that the alloying elements Al and Zn tend to have a stabilizing effect on the protective film formed on Mg alloy. Indeed, without these alloying elements, pure magnesium experiences a much faster biodegradation under similar testing conditions

[Song & Song, 2007]. The previous electrochemical results show that the corrosion resistance of AZ31 is much higher than that of AZ91 alloy. The results may be caused by the different distribution of alloying elements in microscopic scale and the microstructure of alloys, which are the fundamental reasons for the metal corrosion morphology and corrosion resistance.

In the literature [Ballerini et al., 2005], it was found that the heterogeneous microstructure of AZ91 stimulates a localized corrosion morphology that is dictated by the distribution of microgalvanic coupling with the $Mg_{17}Al_{12}$ intermetallic particles in the matrix. The content of Al in the second-phase particles [Azza et al., 2010] might be the β phase (Mg_{17} Al_{12}), the electrode potential of the β phase is higher than the matrix; therefore, it will form microcells with the adjacent matrix and accelerate the corrosion process. Because the Al content in AZ91 is higher than that of AZ31, the content of β phase of AZ91 will be higher than that of AZ31 and the number of corrosion microcells of AZ91 is also larger than that of AZ31, as a result, the corrosion resistance of AZ91 is lower than that of AZ31.

The corrosion behavior of the Mg alloys is determined by the important aspects include composition, porosity, grain size, and amount and distribution of β phase. Fig. 11 represents the surface morphologies of AZ91 and AZ31 magnesium alloys, the microstructure of AZ31 magnesium alloy shows a nearly continuous network of grain boundary phase ($Mg_{17}Al_{12}$). However, AZ91 contains a few amounts of β-phase. The phase was more stable in NaCl and was more inert to corrosion. The phase corrodes due to the tendency for the corrosion rate of the β-phase to be accelerated by microgalvanic coupling between the α-phase and the β-phase. The phase mainly served as a galvanic cathode and accelerated the corrosion process of the matrix if the volume fraction of β-phase was small; however, for a high volume fraction, the phase might act as an anodic barrier to inhibit the overall corrosion of the alloy. Song et al [Song & Atrens, 1999, 2003 & 2007] showed that the β phase plays a dual role, it can act either as a barrier or as a galvanic anode depending on its content, size and distribution. When the mass fraction of (Mg_{17} Al_{12}) β phase is high, the grain size of magnesium alloy is small, and the β phase distributes continuously on the matrix a phase, so it may play the role of a barrier layer to deter corrosion as shown in the Figure for AZ31. On the contrary, if the grain size is larger and the distance between β phases is enlarged, galvanic corrosion may occur and cause the decline of the corrosion resistance (for AZ91).

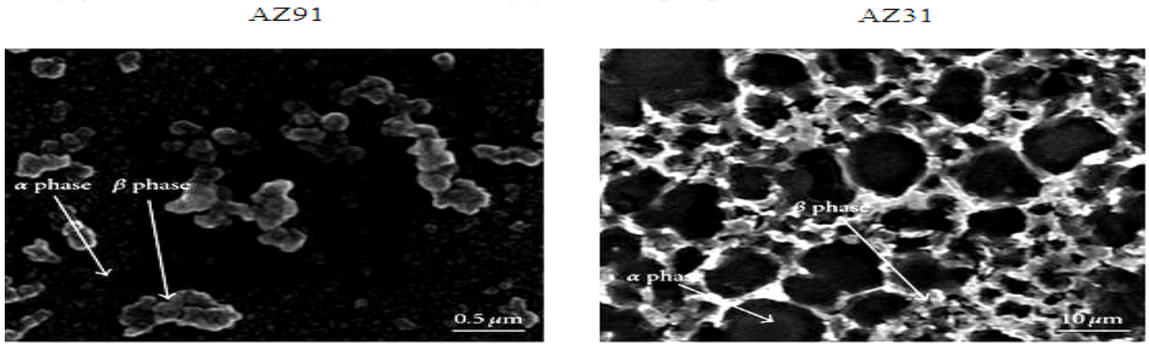

Fig. 11. Surface morphologies of AZ91 and AZ31 magnesium alloys.

Glucosamine is an amino-monosaccharide produced in the body. Glucosamine sulphate acts mainly as a substrate for biosynthesis of mucopolysaccharides and biopolymers of joints and bones and, thus, contributes to restoration of damaged cartilage. About 90% of

glucosamine administered orally as a glucosamine salt gets absorbed from the small intestine and from there it is transported to the liver. Healthy men have serum glucosamine concentration of 0.04 mmol/L when they are not consuming supplemental glucosamine [Ghoneim et al., 2010]. Ingestion of recommended oral doses of glucosamine in humans achieves serum levels of approximately 0.06 mmol/L [Anderson et al., 2005], its oral administration at very large doses (5000–15,000 mg/kg body weight) is well tolerated without documented toxicity. It is not presently known how much of an ingested dose is taken up in the joints in humans. Most relevant clinical trials have used glucosamine sulphate in 1500mg, once a day for 12 weeks [Giordano et al., 2009], this is a prescription drug in most European and non-European countries.

Thus, it is intended in this part to study the effect of adding glucosamine sulphate to Hank's solution on the electrochemical behavior of the biodegrable AZ31 alloy, which is much better than AZ91 alloy against corrosion. Fig. 12 Shows EIS results probed after 4h immersion in Hank's solution in presence of various concentrations of glucosamine sulphate in the range from 0.01 to 10 mM, and presented as Bode and Nyquist plots, the spectra are dominated by the capacitance of the HF time constant. The general features of the plots are not substantially different from those obtained in absence of glucosamine. This suggests that the presence of glucosamine in the solution do not alter the reaction responsible for corrosion. The Nyquist format in Fig. 12 confirms the presence of two well defined depressed semicircles at high and medium frequency regions. In all solutions the impedance, |Z| value decrease with increasing added glucosamine concentration, however the 10 mM shows a critical concentration which has higher resistance compared to that of 1.0 and 0.1 mM glucosamine solution. However, 0.01 mM Glucosamine concentration is much better than 10 mM concentration.

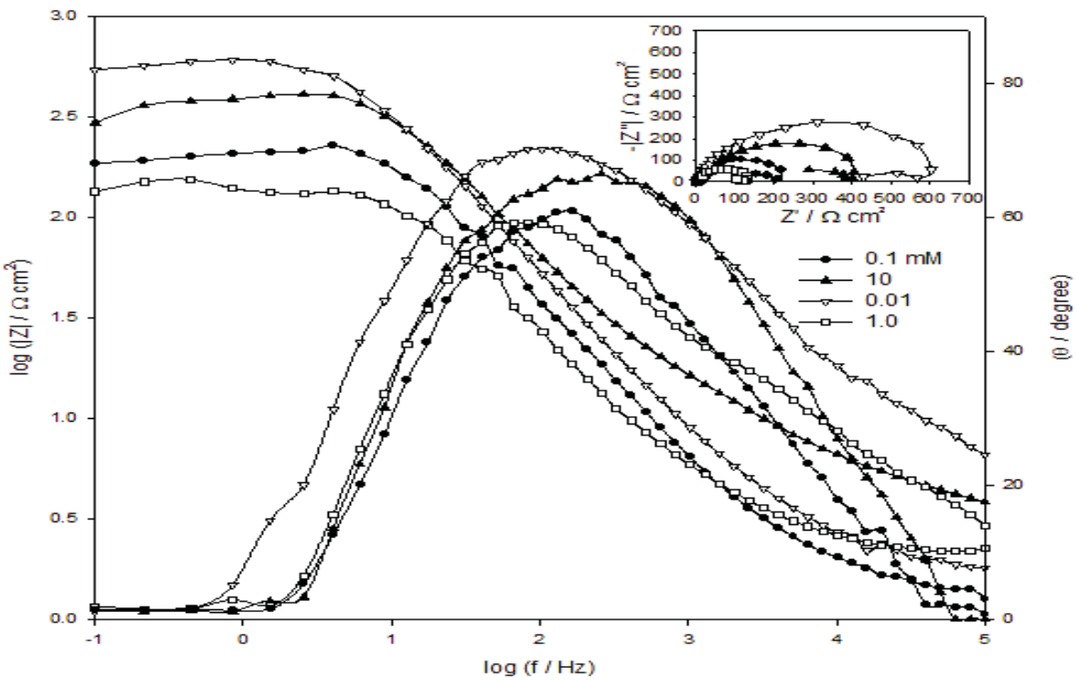

Fig. 12. Bode and Nyquist plots of AZ31E alloy as a function of concentration for Glucosamine in Hank's solution at 37 °C.

The total resistance (R_T) and the relative thickness ($1/C_T$) for AZ31 alloy in Hank's solution in presence of 10 and 0.01 mM glucosamine solutions as a function of the immersion time are presented in Fig. 13. The impedance data were simulated to the equivalent circuit represented in Fig. 2b. Both values increase with immersion time. Also, the total resistance R_T and the relative thickness $1/C_T$ of the film formed on the alloy show always higher values compared to the values in absence of glucosamine as illustrated in Fig. 13.

This was confirmed by Scanning electron microscope (SEM) images shown in Fig. 14a-c. Fig. 14c shows a smoother film adsorbed on the alloy surface for 0.01 mM than that formed on 10 mM concentration Fig. 14b. Also the two are much better than the blank shown in Fig. 14a.

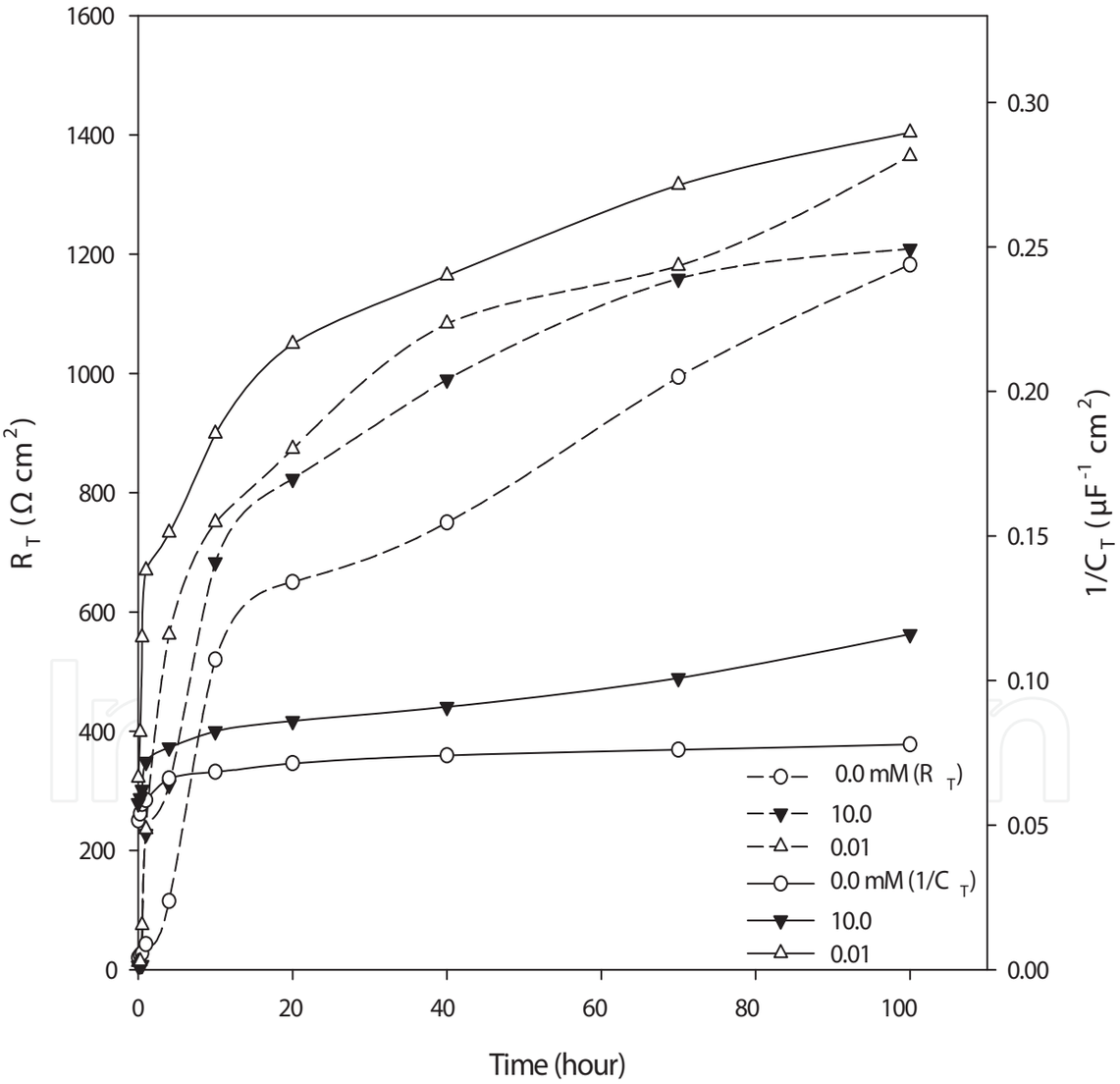

Fig. 13. The total resistance (R_T) and relative thickness ($1/C_T$) for AZ31E alloy with and without Glucoseamine as a function of immersion time in Hank's solution at 37 °C.

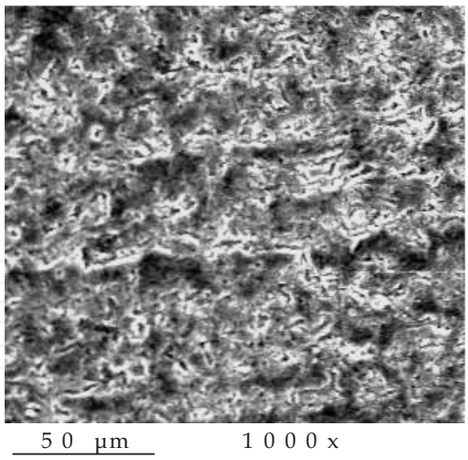

(a) after 100 h immersion in Hank's solution

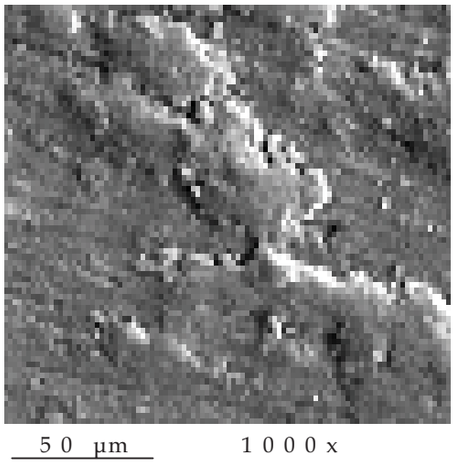

(b) after 100 h immersion in 10 mM Glucosamine containing Hank's solution

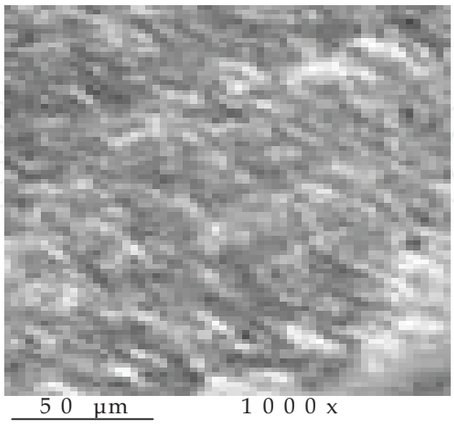

(c) after 100 h immersion in 0.01 mM Glucosamine containing Hank's solution

Fig. 14. SEM micrographs for AZ31E alloy after 100 h of immersion in Hank's solution (a) without Glucosamine (b) with 10 mM Glucosamine and (c) with 0.01 mM Glucosamine.

4.2 Potentiodynamic measurements

Anodic dissolution and passivation behavior of AZ91 and AZ31 alloys were studied in Hank's solution using potentiodynamic polarization measurements (Fig. 14) at a scan rate of 1.0 m V s^{-1}. Prior to the potential scan the electrode was left under open circuit conditions in the respective solution for 100 h until a steady free corrosion potential value was recorded. Basically, the two alloys exhibit the same curve shape, no active-passive transition peak can discerned in the anodic trace, but a passivation plateau extending to a large domain of potential is observed. The corrosion potential (E_{corr}) and corrosion current density (i_{corr}) were calculated from the intersection of the anodic and cathodic Tafel lines extrapolation. The values of i_{corr} were 0.01 and 0.58 mA cm^{-2} for AZ31 and AZ91 respectively. It can be acquired from these experiments that the corrosion resistance of AZ31 alloy is much higher than AZ91. This means that AZ31 has a superior anticorrosion performance in Hank's solution.

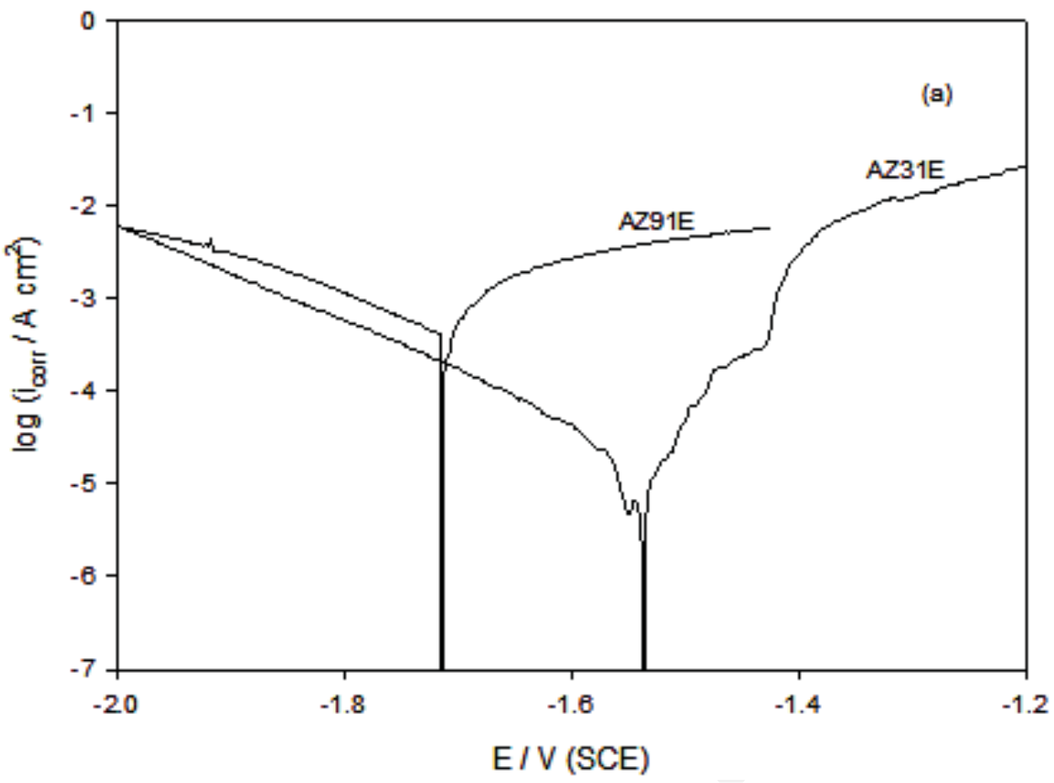

Fig. 15. Potentiodynamic polarization curves for AZ91E and AZ31E alloys in Hank's solution, at 37 ^{o}C .

Figure 16 shows the anodic and cathodic scans of AZ31 alloy immersed for 100 h in Hank's solution in absence and in presence of various concentrations of glucosamine sulphate in the range from 0.01 to 10 mM. The polarization curves reveal clearly that the solution concentration affects both the cathodic and anodic overpotentials, where there is a remarkable shift in the position of the Tafel plots mainly towards more positive values with

decreasing glucosamine concentration. However, 10 mM glucosamine is considered as a critical concentration. The calculated values of i_{corr} were 0.005, 0.003, 0.001 mA/cm^2 for 0.1 mM, 10 mM, 0.01mM glucosamine solution, respectively. These results indicate that addition of glucosamine had a pronounced inhibition effect on the corrosion current, it acts by merely blocking the reaction sites of the metal surface without changing the anodic and cathodic reaction mechanisms. This inhibition is attributed to strong adsorption of molecular species through the active centers as NH_3^+ and OH^- or oxygen heteroatom [Fekry & Mohamed, 2010]. It has been observed that adsorption mainly depends on the presence of π-electrons in C=C, electron pairs on heteroatoms as oxygen or nitrogen, which induce greater adsorption of glucosamine onto the surface of the alloy.

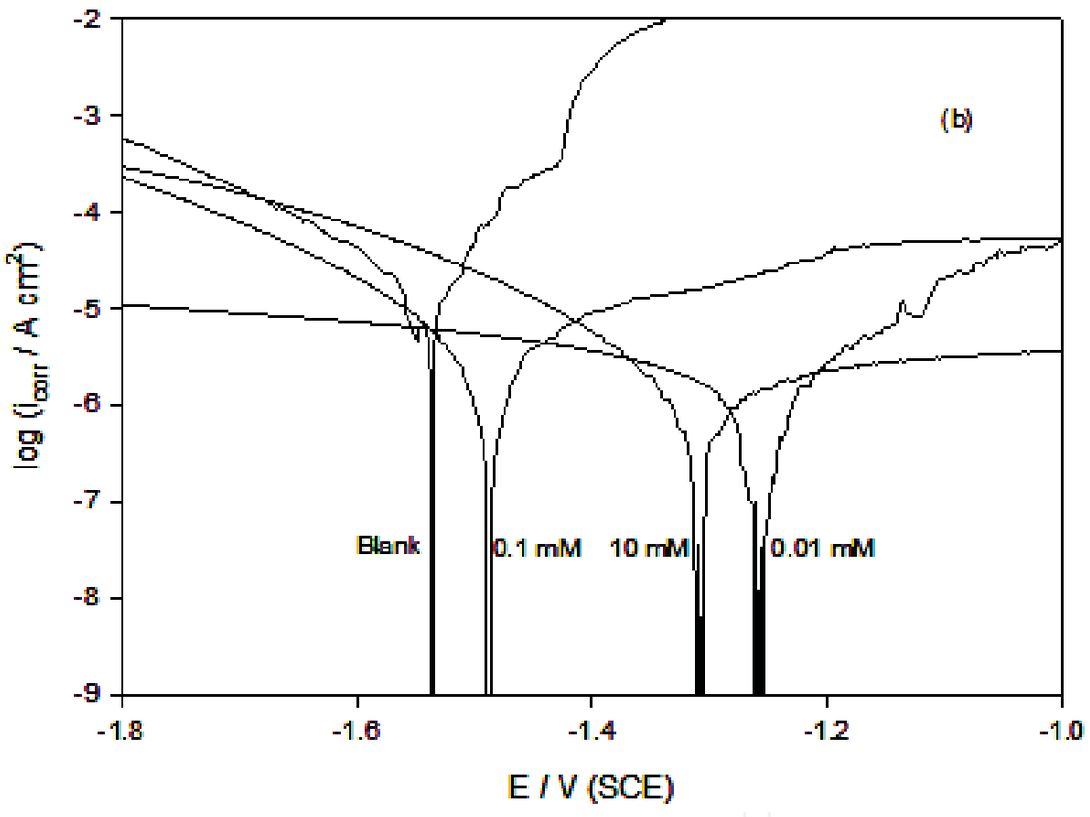

Fig. 16. Potentiodynamic polarization curves for AZ31E alloy as a function of concentration of glucosamine in Hank's Solution at 37 °C .

Generally, the polarization results are in agreement with those obtained from EIS, and suggest that the quality of the spontaneously formed film, as a protective layer against corrosion, improves greatly at lower glucosamine concentration. Finally, for magnesium alloys to be used as biodegradable implant materials, their degradation rates should not exceed the rate of healing of the affected tissue, and also the degradation products should not be more than the body's acceptable absorption level. The present study has shown that the

biodegradation rate of alloy AZ31 in Hank's solution can be significantly reduced by adding glucosamine sulphate to the solution on the basis of the observed corrosion retardation.

5. Conclusions

This work reviews the biological performance of magnesium based alloys (biodegradable materials for temporary implant) as AZ91D alloy in simulated body fluid (SBF), AZ31E alloy in Ringer's and AZ31E, AZ91E in Hank's solution at 37 ^{o}C that have been used as orthopedic biomaterials. Their corrosion behavior was studied by the analysis of corrosion resistance variation with immersion time, using electrochemical impedance spectroscopy (EIS) tests and corrosion current density using potentiodynamic polarization technique. The results were confirmed by scanning electron micrographs.

The aim is to explore possible routes to improve limiting factors such as the corrosion resistance and improve integration of the implant with tissue, and ultimately highlights the need for further research. It is aimed to find the best magnesium alloy with low cost and low corrosion rate as implant in human body. Furthermore, the feasibility to slow down the biodegradation (i.e. corrosion) of magnesium alloys to solve the rapidly corroding magnesium implant problems was demonstrated by studying the effect of adding glucosamine sulphate to Hank's solution on the corrosion behavior of AZ31 alloy.

It was observed that:

1. The corrosion resistance for AZ91D in Simulated body fluid increase with increasing time of immersion until 35 h. It was found to be better than the blank (AZ91D alloy before immersion). It was found that film healing and thickening (increasing R_T value) becomes effective by increasing time of immersion in SBF solution leading to a quasi-steady state thickness at longer times. Generally, SBF improves slightly the corrosion resistance of AZ91D alloy with time.
2. Corrosion resistance found to increase for AZ31E in Ringer's solution with increasing immersion time till 100 h. This is caused by the formation of adherent corrosion products on the sample surface as $Mg(OH)_2$ which is precipitated from the solution during the corrosion of magnesium alloys due to saturation and localized alkalization. This is confirmed by measuring the pH of Ringer's solution after completing the experiment, which becomes 11.0. Also, Ca could improve both the corrosion resistance in NaCl solution and the mechanical properties of magnesium alloy, it is a major component in human bone and can accelerate the bone growth. The growth of the polarization resistance with the immersion time is consistent with the continual decrease of the bio-corrosion rate.
3. The corrosion resistance of AZ91E and AZ31E alloys increase with immersion time in Hank's solution for 100 h. However, the corrosion resistance of AZ31E alloy is much better than AZ91E alloy at all times of immersion.
4. All results are confirmed by scanning electron micrographs and potentiodynamic polarization tests. Thus, AZ31E was found to be the best alloy.
5. By addition of Glucosamine as inhibitor for corrosion of AZ31E in Hank's solution, it was evaluated that total resistance R_T or relative thickness $1/C_T$ of the film formed are higher compared to the values in absence of glucosamine. However, the best corrosion inhibition is observed by addition of 0.01 mM Glucosamine and this was confirmed by SEM images.

6. Thus, AZ31E alloy can be used as temporary implant in human body. It is low in its cost and will dissolve after a time that is the bone become healed. It doesn't need to do another surgery to remove it from human body; it is non-toxic to human body. Thus, Mg alloy can gradually be dissolved and adsorbed after implanting.
7. The previous electrochemical results show that the corrosion resistance of AZ31 is much higher than that of AZ91 alloy. The results may be caused by the different distribution of alloying elements in microscopic scale and the microstructure of alloys, which are the fundamental reasons for the metal corrosion morphology and corrosion resistance.

6. References

Anderson, J.; Nicolosi, R. & Borzelleca, J. (2005). Glucosamine effects in humans: a review of effects on glucose metabolism, side effects, safety considerations and efficacy. Food and Chemical Toxicology, Vol. 43, No. 2, (February 2005), Pages (187-201), ISSN: 0278-6915.

Ballerini, G.; Bardi, U.; Bignucolo, R. & Ceraolo, G. (2005). About some corrosion mechanisms of AZ91D magnesium alloy. Corrosion Science, Vol. 47, No. 9, (September 2005), Pages (2173-2184), ISSN: 0010-938X.

a. Fekry, A. (2009). The influence of chloride and sulphate ions on the corrosion behavior of Ti and Ti-6Al-4V alloy in oxalic acid. Electrochimica Acta, Vol. 54, No. 12, (30 April 2009), Pages (3480-3489), ISSN: 0013-4686.

b. Fekry, A. & El-Sherief, R. (2009). Electrochemical corrosion behavior of magnesium and titanium alloys in simulated body fluid. Electrochimica Acta, Vol. 54, No. 28, (1 December 2009), Pages (7280-7285), ISSN: 0013-4686 .

c. Fekry, A & Mohamed, R. (2010). Acetyl thiourea chitosan as an eco-friendly inhibitor for mild steel in sulphuric acid medium. Electrochimica Acta, Vol. 55, No. 6, (15 February 2010), Pages (1933-1939), ISSN: 0013-4686.

Ghoneim, A.; Fekry, A. & Ameer, A. Electrochemical behavior of magnesium alloys as biodegradable materials in Hank's solution. Electrochimica Acta, Vol. 55, No. 20, (1 August 2010), Pages (6028-6035), ISSN: 0013-4686.

Giordano, N.; Fioravanti, A.; Papakostas, P.; Montella, A.; Giorgi, G. & Nuti, R. (2009). The efficacy and tolerability of glucosamine sulfate in the treatment of knee osteoarthritis: A randomized, double-blind, placebo-controlled trial. Current Therapeutic Research, Vol. 70, No. 3. (June 2009), pages (185-196), ISSN: 0011-393X.

Gu, X.; Zheng, Y.; Cheng, Y.; Zhong, S. & Xi, T. (2009). In vitro corrosion and biocompatibility of binary magnesium alloys. Biomaterials, Vol. 30, No. 4, (February 2009), Pages (484-498). ISSN: 0142-9612.

a. Heakal, F.; Fekry, A. & Fatayerji, M. (2009). Electrochemical behavior of AZ91D magnesium alloy in phosphate medium—part I. Effect of pH. Journal of Applied Electrochemistry, Vol. 39, No. 5 (May 2009), pages (583-591), ISSN: 0021-891X.

b. Heakal, F.; Fekry, A. & Fatayerji, M. (2009). Electrochemical behavior of AZ91D magnesium alloy in phosphate medium: Part II. Induced passivation. Journal of

Applied Electrochemistry, Vol. 39, No. 9, (September 2009), pages (1633-1642), ISSN: 0021-891X.

c. Heakal, F.; Fekry, A. & Fatayerji, M. (2009). Influence of halides on the dissolution and passivation behavior of AZ91D magnesium alloy in aqueous solutions. Electrochimica Acta, Vol. 54, No. 5, (February 2009), Pages (1545-1557), ISSN: 0013-4686.

Jönsson, M.; Persson, D. & Thierry, D. (2007). Corrosion product formation during NaCl induced atmospheric corrosion of magnesium alloy AZ91D. Corrosion Science, Vol. 49, No. 3, (March 2007), Pages (1540-1558), ISSN: 0010-938X.

Kainer, K.; Buch, F. (2003). Chapter 1: The Current State of Technology and Potential for Further Development of Magnesium Applications, In: Magnesium-Alloys and Technology. Kainer, k. (June 2003), pages (1-22), Wiley-VCH Verlag GmbH & Co. KG aA, Weinheim (2003). ISBN: 9783527305704, Germany.

Mani, G.; Feldman, M.; Patel, D. & Agrawal, M. (2007). Coronary stents: A materials perspective. Biomaterials, Vol. 28, No. 9, (March 2007), Pages (1689-1710), ISSN: 0142-9612.

Narayanan, R. & Seshadri, S. Phosphoric acid anodization of Ti–6Al–4V–Structural and corrosion aspects Corrosion Science, Vol. 49, No. 2, (February 2007), Pages (542-558), ISSN: 0010-938X.

Pardo, A.; Merino, M.; Coy, A.; Arrabal, R.; Viejo, F. & Matykina, A. (2008). Corrosion behaviour of magnesium/aluminium alloys in 3.5 wt.% NaCl. Corrosion Science, Vol. 50, No. 3, (March 2008), Pages (823-834), ISSN: 0010-938X.

Revell, P.; Damien, E.; Zhang, X.; Evans, P. & Howlett, C. (2004). The effect of magnesium ions on bone bonding to hydroxyapatite coating on titanium alloy implants, Key Eng. Mater. 254 (2004) 447–450.

Staiger, M.; Pietak, A.; Huadmai, J. & Dias, G. (2006). Magnesium and its alloys as orthopedic biomaterials: A review Biomaterials, Vol. 27, No. 9, (March 2006), Pages (1728-1734), ISSN: 0142-9612.

a. Song, G.; Atrens, A; St John, D.; Wu, X. & Nairn, J. (1997). The anodic dissolution of magnesium in chloride and sulphate solutions. Corrosion Science, Vol. 39, No. 10-11, (October-November 1997), Pages (1981-2004), ISSN: 0010-938X.

b. Song, G.; Atrens, A & Dargusch, M. (1998). Influence of microstructure on the corrosion of diecast AZ91D Corrosion Science, Vol. 41, No. 2, (February 1998), Pages (249-273), ISSN: 0010-938X.

c. Song, G. & Atrens, A. (2003). Understanding magnesium corrosion. A framework for improved alloy performance. Advanced Engineering Materials, Vol. 5, No. 12, (December 2003), Pages (837-858), ISSN: 1438-1656.

d. Song, G. (2005). Recent progress in corrosion and protection of magnesium alloys. Advanced Engineering Materials, Vol. 7, No. 7, (July 2005), Pages (563-586), ISSN: 1438-1656.

e. Song, G. & Atrens, A. (2007). Recent Insights into the Mechanism of Magnesium Corrosion and Research Suggestions. Advanced Engineering Materials, Vol. 9, No. 3, (March 2007), Pages (177-183), ISSN: 1438-1656.

f. Song, G. (2007). Control of biodegradation of biocompatable magnesium alloys. Corrosion Science, Vol. 49, No. 4, (April 2007), Pages (1696-1701), ISSN: 0010-938X.

g. Song, G. & Song, S. (2007). A Possible Biodegradable Magnesium Implant Material. Advanced Engineering Materials, Vol. 9, No. 4, (April 2007), Pages (298-302), ISSN: 1438-1656.

Wang, H.; Estrin, Y. & Zúberová, Z. (2008). Bio-corrosion of a magnesium alloy with different processing histories. Materials Letters, Vol. 62, No. 16, 15, (June 2008), Pages (2476-2479), ISSN: 0167-577X.

a. Witte, F.; Kaese, V.; Switzer, H.; Meyer-Lindenberg, A.; Wirth, C. & Windhagen, H. (2005). In vivo corrosion of four magnesium alloys and the associated bone response. Biomaterials, Vol. 26, No. 17, (June 2005), Pages (3557-3563), ISSN: 0142-9612.

b. Witte, F.; Fisher, J.; Nellesen, J.; Crostack, H.; Kaese, V.; Pisch, A.; Beckmann, F. & Windhagen, H. (2006). In vitro and in vivo corrosion measurements of magnesium alloys. Biomaterials, Vol. 27, No. 7, (March 2006), Pages (1013-1018), ISSN: 0142-9612.

c. Witte, F.; Hort, N.; Vogt, C.; Cohen, S.; Kainer, K.; Willumeit, R. & Feyerabend, F. (2008). Degradable biomaterials based on magnesium corrosion. Current Opinion in Solid State and Materials Science, Vol. 12, No. 5-6, (October-December 2008), Pages (63-72), ISSN: 1359-0286.

Wu, G.; Fan, Y.; Atrens, A.; Zhai, C. & Ding, W. (2008). Electrochemical behavior of magnesium alloys AZ91D, AZCe2, and AZLa1 in chloride and sulfate solutions. Journal of Applied Electrochemistry, Vol. 38, No. 2, (February 2008), pages (251-257), ISSN: 0021-891X.

Yamasaki, Y.; Yoshida, Y.; Okazaki, M.; Shimazu, A.; Uchida, T. & Kubo,T. (2002). Synthesis of functionally graded MgCO3 apatite accelerating osteoblast adhesion. Journal of Biomedical Materials Research, Vol. 62, No. 1, (October 2002), pages (99–105), ISSN: 1549-3296.

Yamasaki, Y.; Yoshida, Y.; Okazaki, M.; Shimazu, A.; Kubo, T. & Akagawa, Y. (2003). Action of FGMgCO3Ap-collagen composite in promoting bone formation. Biomaterials, Vol. 24, No. 27, (December 2003), Pages (4913-4920), ISSN: 0142-9612.

Zenner, H. & Renner, F. (2002). Cyclic material behavior of magnesium die castings and estrusions. International journal of Fatigue, Vol. 24, No. 12, (December 2002), pages (1255-1260), ISSN: 0142-1123.

Zhang, E.; Yin, D.; Xu, L.; Yang, L. & Yang, K. (2009). Microstructure, mechanical and corrosion properties and biocompatibility of Mg–Zn–Mn alloys for biomedical application. Materials Science and Engineering: C, Vol. 29, No. 3, (30 April 2009), Pages (987-993), ISSN: 0928-4931.

Zreiqat, H.; Howlett, C.; Zannettino, A. & Evans, P. (2002). Mechanisms of magnesium stimulated adhesion of osteoblastic cells to commonly used orthopaedic implants. Journal of Biomedical Materials Research, Vol. 62, No. 2, (November 2002), Pages (175-184), ISSN: 1549-3296.

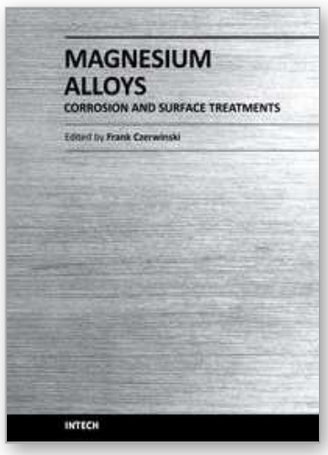

Magnesium Alloys - Corrosion and Surface Treatments

Edited by Frank Czerwinski

ISBN 978-953-307-972-1
Hard cover, 344 pages
Publisher InTech
Published online 14, January, 2011
Published in print edition January, 2011

A resistance of magnesium alloys to surface degradation is paramount for their applications in automotive, aerospace, consumer electronics and general-purpose markets. An emphasis of this book is on oxidation, corrosion and surface modifications, designed to enhance the alloy surface stability. It covers a nature of oxides grown at elevated temperatures and oxidation characteristics of selected alloys along with elements of general and electrochemical corrosion. Medical applications are considered that explore bio-compatibility of magnesium alloys. Also techniques of surface modifications, designed to improve not only corrosion resistance but also corrosion fatigue, wear and other behaviors, are described. The book represents a valuable resource for scientists and engineers from academia and industry.

How to reference

In order to correctly reference this scholarly work, feel free to copy and paste the following:

Amany Fekry (2011). Electrochemical Corrosion Behavior of Magnesium Alloys in Biological Solutions, Magnesium Alloys - Corrosion and Surface Treatments, Frank Czerwinski (Ed.), ISBN: 978-953-307-972-1, InTech, Available from: http://www.intechopen.com/books/magnesium-alloys-corrosion-and-surface-treatments/electrochemical-corrosion-behavior-of-magnesium-alloys-in-biological-solutions

INTECH
open science | open minds

InTech Europe
University Campus STeP Ri
Slavka Krautzeka 83/A
51000 Rijeka, Croatia
Phone: +385 (51) 770 447
Fax: +385 (51) 686 166
www.intechopen.com

InTech China
Unit 405, Office Block, Hotel Equatorial Shanghai
No.65, Yan An Road (West), Shanghai, 200040, China
中国上海市延安西路65号上海国际贵都大饭店办公楼405单元
Phone: +86-21-62489820
Fax: +86-21-62489821

IntechOpen